Neutral Dissociation of Superexcited Oxygen Molecules in Intense Laser Fields†

Di Song,‡ Ali Azarm,§ Yousef Kamali,§ Kai Liu,‡ Andong Xia,‡ Yoshiaki Teranishi,∥,⊥ Sheng-Hsien Lin,*,∥,⊥ Fanao Kong,*,‡ and See Leang Chin*,§

Institute of Chemistry, Chinese Academy of Science, Beijing 100190, People's Republic of China, Department of Physics, Engineering Physics and Optics & Center for Optics, Photonics and Laser (COPL), Université Laval, Québec City, Québec, G1 V 0A6, Canada, Institute of Atomic and Molecular Science, Academia Sinica, P.O. Box 23-166, Taipei, Taiwan, Republic of China, and Institute of Applied Chemistry, Institute of Molecular Science, Chiao-Tung University, Hsin-Chu, Taiwan, Republic of China

Received: August 8, 2009; Revised Manuscript Received: November 23, 2009

Superexcited states (SESs) of oxygen molecules and their neutral dissociation processes have been studied both experimentally and theoretically using intense femtosecond laser. We find that at the laser intensity of $\sim 2 \times 10^{14}$ W/cm^2, ultrashort laser pulse causes neutral dissociation of oxygen molecule by way of SESs. The dissociation products are the excited neutral oxygen atoms, which are observed through fluorescence spectroscopy. Laser power dependence of the fluorescence intensity shows that each molecule effectively absorbs an average of ten laser photons. The total energy absorbed is sufficient to stimulate the molecule to many of the SESs. The effect is equivalent to single photon excitation in the extreme-ultraviolet (XUV) region by synchrotron radiation (SR). Morse potential energy curves (PECs) are constructed for the SESs of O_2 molecules. In light of the PECs, predissociation mechanism is proposed for the neutral dissociation. Quasi-classical trajectory (QCT) calculations show that the predissociation time is as short as 100 fs, which is consistent with our experimental measurement using ultrafast pump−probe technique.

1. Introduction

Superexcited states (SESs) of molecules have attracted much attention in recent years. SES is a highly excited state of a molecule, whose excitation energy is more than the first ionization potential (IP) energy of the molecule. The term "superexcited state of a molecule" was first coined by Hurst and emphasized by Platzman.[1−3] Later, Hatano noted that "most observed SESs are assigned to Rydberg states that are vibrationally (or/and rotationally), doubly, or inner core exited and converge to each of ion states".[4,5] So far, it is known that SES occurs widely when a molecule is impacted by high energy particles or irradiated by vacuum-ultraviolet (VUV) light, X-rays, or γ rays. SESs are unstable, undergoing decay rapidly. The decay processes include autoionization, ion pair dissociation, and neutral dissociation. Understanding the essence and the decay processes of SES is of importance for radiation chemistry, photochemistry, upper atmospheric physics, and astrophysics.[6−15] However, the dissociation mechanism is obscure and needs to be explored since the dissociative potential energy surface (PES) of the SES is absent in the literature.

Studies of SESs of O_2 molecules can be treated as a typical example. Ukai et al.[16] and Karawajczyk et al.[17] investigated neutral dissociation of SES in the energy region of 14−21 eV by using synchrotron radiation (SR) as a conventional excitation method. They roughly assigned several excited O atoms observed in their excitation spectra to dissociation products in Rydberg states converging to the B ($^2\Sigma_g^-$), b ($^4\Sigma_g^-$), or A ($^2\Pi_u$) states of the O_2^+ ion, respectively, but did not supply enough theoretical explanation of the dissociation mechanism. While Odagiri et al. focused on experimentally indentifying the inner-valence excited states and multiply excited states of O_2 as SESs in the higher energy range of 23−47 eV using the photon−photon coincidence method.[18]

In this work, we study the dissociation processes of the superexcited states of O_2 molecule induced by femtosecond intense laser pulses both theoretically and experimentally. Four issues will be described in this paper. First of all, we report that the thirty-three spectral lines from excited oxygen atoms are the dissociation products of the superexcited oxygen molecules produced in the intense laser field. It indicates that more dissociation channels occur in the intense laser field than those observed in SR excitation. Second, the product yield is strongly dependent on the laser intensity. The strong laser power dependence of the intensities of various fluorescence lines with slopes between 9 and 11 in a log−log plot provides the experimental evidence that the precursor states of excited O atoms should be some SESs of O_2 molecules. The above two issues prove that using a femtosecond intense laser to excite SES is complementary to synchrotron excitation. Although we proved it in the case of CH_4,[11,12] the observation in O_2 starts to indicate that this capability of exciting SES in molecules is a universal process during intense femtosecond laser interaction with molecules. The third issue is that we have constructed empirical (Morse) potential energy curves (PECs) for the SESs of O_2. On the basis of the Morse PECs, we propose a predissociation mechanism to interpret the dissociation processes of SESs. The emissions of products thus could be well explained. These theoretical results can provide a better insight into the essence of SESs than before. Finally, we measured directly the lifetime of the SES and compared it with the quasi-classical trajectory (QCT) calculations. It showed that the neutral

† Part of the "Benoît Soep Festschrift".

* To whom correspondence should be sent. E-mail: F.K., kong@iccas.ac.cn; S.L.C., See.Leang.Chin@copl.ulaval.ca; S.H.L., hcshaw@po.iams.sinica.edu.tw.

‡ Chinese Academy of Science.

§ Université Laval.

∥ Academia Sinica.

⊥ Chiao-Tung University.

10.1021/jp907662z
Published on Web 12/31/2009

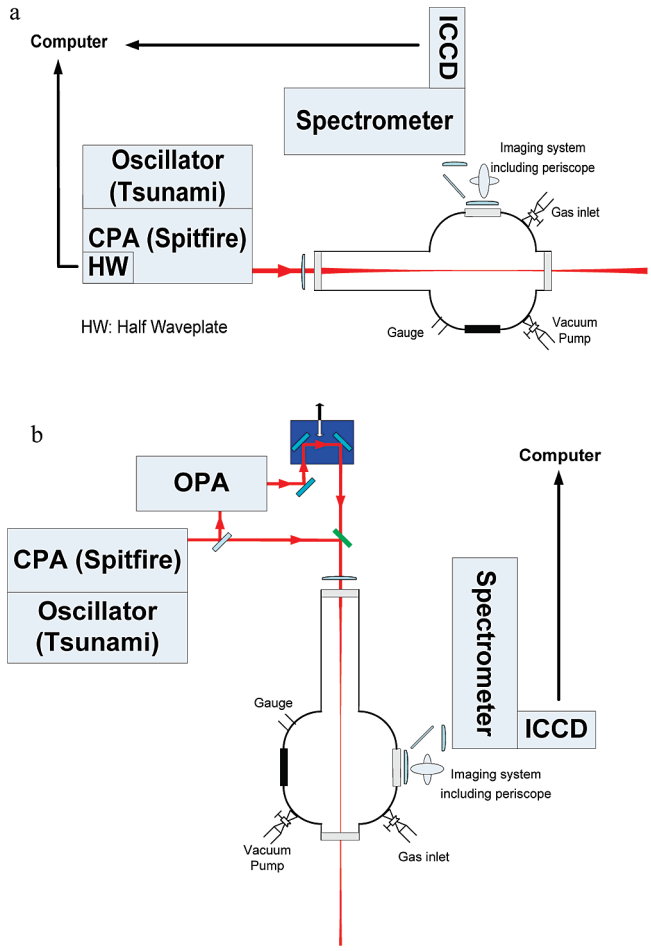

Figure 1. (a) Sketch of the experimental setup to obtain fluorescence spectra and the variation of some lines versus intensity. (b) Sketch of the pump and probe experimental setup.

dissociation of a SES is indeed a fast predissociation process. Through the above studies, the concept of the SES of O_2 molecule and the mechanism of the dissociation are better clarified.

2. Experimental Setup

A schematic diagram of our experimental setup to obtain the fluorescence spectra and the variation of some lines versus intensity is illustrated in Figure 1a. The seed pulses from a femtosecond Ti−sapphire oscillator (Spectra Physics Tsunami) is sent into a chirp pulse amplification (CPA) module (Spectra Physics Spitfire). In the CPA section, first, a stretcher is used to stretch the pulses from 30 fs near transform limited to around 200 ps positively chirped pulses. Then two Ti−sapphire amplifier systems, a regenerative amplifier followed by a two-pass amplifier, increases the energy of the stretched seed pulses. Finally, a parallel grating compressor is used to give a transform-limited pulse with pulse duration of about 42 fs at fwhm (full width at half-maximum). The pulse duration is measured using a second-order single-shot autocorrelator (SSA, Positive Light). The output beam has 1 kHz repetition rate, maximum energy of 2 mJ/pulse with a diameter of about 5 mm (1/e2 level of intensity). A half-wave plate is used before the compressor to change the energy of the pulses.

The sketch of pump and probe experimental setup is illustrated in Figure 1b. The slightly negative chirped pulse from spitfire is optimized for the optical parametric amplifier (OPA 800C Spectra Physics) system. The laser beam is then separated into two arms by a 50/50 beam splitter. One was used as the pump beam (~900 μJ/pulse). The other is sent to an OPA to generate the infrared probe pulses at 1338 nm with a pulse duration of about 50 fs (fwhm) and a pulse energy around 65 μJ. In the probe arm, a high resolution delay line (40 nm) is used to collect the data versus the different delay time between pump and probe pulses. The probe beam had a horizontal polarization parallel to that of the pump beam. Both of the laser beams are focused into a vacuum chamber with the same lens. Spatial superposition of the two pulses is checked with a far-field measurement, while temporal superposition of these two pulses in air is checked by a four wave mixing (4WM) process, where two photons of 800 nm are mixed with one infrared photon ($2\omega_{800} - \omega_{ir}$), leading to a yellowish laser emission.

Finally, in both experiments, the laser pulse is focused into a vacuum chamber by a plano-convex lens ($f = 100$ cm). The vacuum chamber is evacuated by triscroll vacuum pump (Varian Inc.) to the background pressure of 4×10^{-2} Torr. Then pure oxygen (O_2 Praxair Inc.) was introduced to the interaction chamber at an equilibrium pressure of 10 Torrs.

The collected fluorescence from the interaction zone is delivered to the spectrometer (Acton research Coorporation, SpectraPro 500i) entrance slit with 100 μm slit width. We use an imaging system including a metallic-mirrors periscope and a fused silica lenses to image the fluorescence signal into the spectrometer. The spectrometer is operated with either a 1200 or 2400 groove/mm grating for the higher spectral resolution. The selected wavelength with the proper grating inside the spectrometer is detected by an Intensified Charged Coupled Devices (ICCD) camera (Princeton Instrument ICCD PIMAX 512). We use a gating mode to get rid of the scattered signal coming from the main pulses. Gate delay is chosen to be around of 50 ns the after arrival time of main pulse in the interaction zone and the gate width is 500 ns.

3. Results and Discussion

3.1. Fluorescence Spectrum and Dissociation Products.

3.1.1. Emission Spectrum. We reported previously that in a strong laser field of 2×10^{14} W/cm^2, polyatomic molecules of methane, ethylene, *n*-butane, and 1-butene undergo neutral fragmentation with characteristic fluorescence.[11,12] The fragmentation takes place in the SESs of the molecules. In the present study, the neutral dissociation of the superexcited diatomic molecule, O_2, is investigated. The SESs are produced by the intense Ti:sapphire laser pulses. Products of the neutral dissociation are detected by fluorescence spectroscopy. Figure 2a shows the fluorescence spectrum recorded between the wavelengths of 300 and 900 nm. Dissociation of the SESs of O_2 molecules in an intense laser field is significant. It reveals that the SESs can also be created by intense laser excitation. It is an alternative method to produce the SESs of molecules, in addition to SR excitation.

The emission bands between 306 and 320 nm are assigned to the rovibronic transitions of O_2^+ ($A\ ^2\Pi \rightarrow X\ ^2\Pi$),[19] which are not dealt with in the present paper. The artifacts between 612 and 640 nm are attributed to the second-order diffraction of the same transitions of O_2^+ ($A\ ^2\Pi \rightarrow X\ ^2\Pi$). Similarly, the emissions at 789.7 and 873.8 nm are the second-order diffraction of the spectral lines at 394.8 and 436.8 nm, respectively. The rest of the spectral lines in the spectrum are attributed to the transitions in the oxygen atoms, which are the dissociation products of O_2.

We measure the pressure dependence of fluorescence intensity. Figure 3 shows the integral around 777 nm lines versus

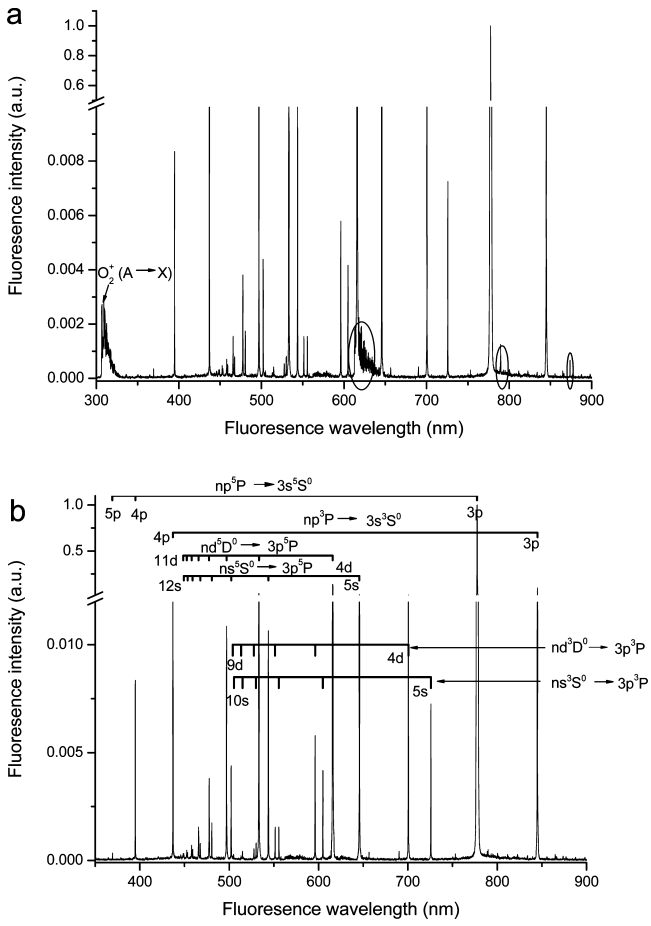

Figure 2. (a) Original fluorescence spectrum of the photodissociation products. The artifacts between 612 and 640 nm are attributed to the second-order diffraction of the same transitions of O_2^+ ($A\ ^2\Pi \rightarrow X\ ^2\Pi$). The emissions at 789.7 and 873.8 nm are the second-order diffraction of the spectral lines at 394.8 and 436.8 nm, respectively. (b) Having deducted the O_2^+ ($A\ ^2\Pi \rightarrow X\ ^2\Pi$) rovibrational bands and artifacts from the entire spectrum (Figure 2a), the fluorescence spectrum of O atom is merely shown.

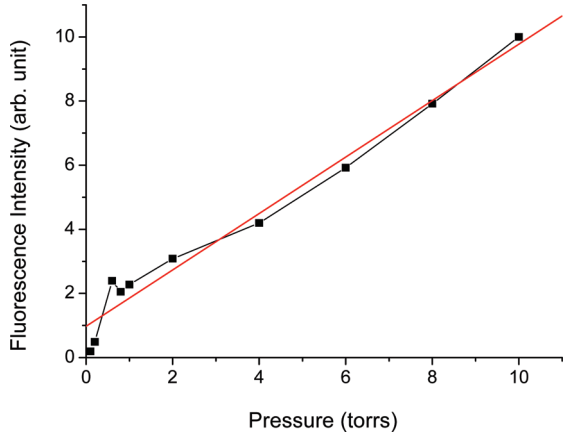

Figure 3. Fluorescence signals around 777 nm versus the pressure varied from 0.1 to 10 Torr.

pressure. The pressure dependence below 10 Torr is linear and the slope is nearly 1, which means the collision effect can be neglected. The linear pressure dependence shows that the emitters are the products of unimolecular dissociation, but not those of bimolecular reactions.

3.1.2. Assignment of Spectral Lines. Thirty-three spectral lines have been recorded in the fluorescence spectrum (Figure 2b). In the last column of Table 1, the observed wavelengths and the wavelengths reported in the literatures are listed. Ten transitions of them are the new observations. The remaining twenty-three transitions can be found in the NIST table.[20] They are assigned to the transitions of six Rydberg series of O atoms. The observed transitions and their assignments are listed in columns 4 and 5 of Table 1. According to ref 20, the transitions are $2s^22p^2(^4S^0)3p$,4p and 5p, $^5P \rightarrow 2s^22p^2(^4S^0)3s$, $^5S^0$ at 777.5, 394.8, and 369.5 nm; $2s^22p^2(^4S^0)3p$ and 4p, $^3P \rightarrow 2s^22p^2(^4S^0)3s$, $^3S^0$ at 845.0 and 436.8 nm; $2s^22p^2(^4S^0)4d\sim8d$, $^5D^0 \rightarrow 2s^22p^2(^4S^0)3p$, ^5P at 615.9, 533.2, 497.1, 477.5, and 465.7 nm; $2s^22p^2(^4S^0)4d\sim8d$, $^3D^0 \rightarrow 2s^22p^2(^4S^0)3p$, ^3P at 700.6, 596.2, 551.4, 527.7, and 513.3 nm; $2s^22p^2(^4S^0)5s\sim8s$, $^5S^0 \rightarrow 2s^22p^2(^4S^0)3p$, ^5P at 645.4, 543.5, 502.2, and 480.4 nm; and $2s^22p^2(^4S^0)5s\sim8s$, $^3S^0 \rightarrow 2s^22p^2(^4S^0)3p$, ^3P at 725.8, 604.9, 555.6, and 530.1 nm, respectively.

The remaining ten transitions marked by triangles in Table 1 have not been reported in the literature. By means of the Rydberg formula, here we verify that these transitions can be assigned to the unreported Rydberg transitions. Referring to these transitions, three new Rydberg states, $2s^22p^2(^4S^0)11s$, $^5S^0$, $2s^22p^2(^4S^0)12s$, $^5S^0$, and $2s^22p^2(^4S^0)$ 10d, $^5D^0$, which have not been reported previously, are observed in this experiment and shown in the Table 1, with the symbol of double triangles.

The oxygen molecule undergoes neutral dissociations in the intense laser field. Most likely, the product pair consists of a ground state oxygen atom O (^3P) and an excited oxygen atom of O (n, l), where n and l are the principle and angular quantum numbers, respectively. A variety of the products found in the spectrum indicate that many dissociation channels exist simultaneously. This indicates also that various SESs of O_2 have been created in the intense laser fields.

3.2. Laser Power Dependence of the Fluorescence Intensity. To understand the dissociation process of the O_2 molecule, we measured the fluorescence intensity of the O atoms as a function of the laser intensity. Three slopes are obtained as 8.9, 11.1, and 11.3 in a log−log plot for the wavelengths of 615.9, 777.5, and 845.0 nm, respectively (Figure 4a). In the view of multiphoton excitation theory, this observation implies that the rate-determining process may absorb at least ten photons (1.55 eV each photon at 800 nm) on average. In other words, the O_2 molecule can be excited to a highly excited state, whose energy (>15.5 eV) is beyond the first ionization potential of 12.0697 eV. The highly excited state, or the superexcited state, then undergoes dissociation leading to the product of O atoms we observed.

We theoretically investigate the multiphoton excitation dynamics of O_2 molecule in strong laser fields. Multiphoton excitations are caused by absorbing a certain number of photons. The slope in the log−log plot suggests the number of the photons involved in the excitation process. The calculation method has been described in detail in a previous paper.[21] Only a brief introduction is given here. We made a quantum chemical calculation with the complete active space self-consistent-field (CASSCF) method with the aug-cc-pVTZ basis set to obtain the excitation energy and transition dipole moment matrix elements between the eigenstates. For O_2, we take 96 valence states into the calculation. The first excitation energy is about 1.0 eV, and the highest eigenstate included has the energy of ~21 eV above the ground state.

Figure 4b shows the calculated transition probabilities of the vertical excitation as functions of laser power for the 96 states. Most of the curves of power dependence have slopes between 9 and 11, which are in good agreement with the experimental

TABLE 1: Excitation Energy, Optically Excited State (OES), Dissociative Excited State (DES), Dissociation Products (O* + O(^{3}P)) and Product Emissions of Each Dissociation Process for SESs of the O_2 Molecule[a]

excitation energy (eV)	SESs		dissociation products	assignments of transitions	emission wavelengths (nm)	
	OES	DES			Observation	ref 20
15.3−17.1	O_2** ((O_2^+ A $^2\Pi_u$) $ns\sigma_g$, $^3\Pi_u$) $n = 4, 5$	O_2**(O_2^+ d $^4\Sigma_g^+$) $3p\sigma_u$, $^3\Sigma_u^+$)	O(3p, ^{5}P)	$2s^22p^2(^4S^0)3p$, $^5P \rightarrow 2s^22p^2(^4S^0)3s$, $^5S^0$	777.5	777.54
			O(3p, ^{3}P)	$2s^22p^2(^4S^0)3p$, $^3P \rightarrow 2s^22p^2(^4S^0)3s$, $^3S^0$	845.0	844.68
17.0−18.0	O_2** ((O_2^+ b $^4\Sigma_g^-$) $np\pi_u$, $^3\Pi_u$) $n = 4, 5$	O_2** ((O_2^+ d $^4\Sigma_g^+$) $3p\sigma_u$, $^3\Sigma_u^+$)	O(3p, ^{5}P)	$2s^22p^2(^4S^0)3p$, $^5P \rightarrow 2s^22p^2(^4S^0)3s$, $^5S^0$	777.5	777.54
			O(3p, ^{3}P)	$2s^22p^2(^4S^0)3p$, $^3P \rightarrow 2s^22p^2(^4S^0)3s$, $^3S^0$	845.0	844.68
		O_2**((O_2^+ d $^4\Sigma_g^+$) $4p\sigma_u$, $^3\Sigma_u^+$)	O(4p, ^{5}P)	$2s^22p^2(^4S^0)4p$, $^5P \rightarrow 2s^22p^2(^4S^0)3s$, $^5S^0$	394.8	394.75
			O(4p, ^{3}P)	$2s^22p^2(^4S^0)4p$, $^3P \rightarrow 2s^22p^2(^4S^0)3s$, $^3S^0$	436.8	436.83
		O_2**((O_2^+ d $^4\Sigma_g^+$) $5p\sigma_u$,$^3\Sigma_u^+$)	O(5p, ^{3}P)	$2s^22p^2(^4S^0)4p$, $^3P \rightarrow 2s^22p^2(^4S^0)3s$, $^3S^0$	369.4	369.34
17.0−18.0	O_2** ((O_2^+ b $^4\Sigma_g^-$) $np\sigma_u$, $^3\Sigma_u^-$) $n = 4, 5$	O_2** ((O_2^+ f $^4\Pi_g$) $3p\sigma_u$, $^3\Pi_u$)	O(3p, ^{5}P)	$2s^22p^2(^4S^0)3p$, $^5P \rightarrow 2s^22p^2(^4S^0)3s$, $^5S^0$	777.5	777.54
			O(3p, ^{3}P)	$2s^22p^2(^4S^0)3p$, $^3P \rightarrow 2s^22p^2(^4S^0)3s$, $^3S^0$	845.0	844.68
		O_2** ((O_2^+ f $^4\Pi_g$) $4p\sigma_u$, $^3\Pi_u$)	O(4p, ^{5}P)	$2s^22p^2(^4S^0)4p$, $^5P \rightarrow 2s^22p^2(^4S^0)3s$, $^5S^0$	436.8	436.83
			O(4p, ^{3}P)	$2s^22p^2(^4S^0)4p$, $^3P \rightarrow 2s^22p^2(^4S^0)3s$, $^3S^0$	394.8	394.75
		O_2** ((O_2^+ f $^4\Pi_g$) $5p\sigma_u$, $^3\Pi_u$)	O(5p, ^{3}P)	$2s^22p^2(^4S^0)4p$, $^3P \rightarrow 2s^22p^2(^4S^0)3s$, $^3S^0$	369.4	369.34
19.0−21.0	O_2**((O_2^+ B $^2\Sigma_g^-$) $np\sigma_u$, $^3\Sigma_u^-$) $n = 4, 5$	O_2** ((O_2^+ f $^4\Pi_g$) $3p\sigma_u$, $^3\Pi_u$)	O(3p, ^{5}P)	$2s^22p^2(^4S^0)3p$, $^5P \rightarrow 2s^22p^2(^4S^0)3s$, $^5S^0$	777.5	777.54
			O(3p, ^{3}P)	$2s^22p^2(^4S^0)3p$, $^3P \rightarrow 2s^22p^2(^4S^0)3s$, $^3S^0$	845.0	844.68
		O_2** ((O_2^+ f $^4\Pi_g$) $4p\sigma_u$, $^3\Pi_u$)	O(4p, ^{5}P)	$2s^22p^2(^4S^0)4p$, $^5P \rightarrow 2s^22p^2(^4S^0)3s$, $^5S^0$	394.8	394.75
			O(4p, ^{3}P)	$2s^22p^2(^4S^0)4p$, $^3P \rightarrow 2s^22p^2(^4S^0)3s$, $^3S^0$	436.8	436.83
		O_2** ((O_2^+ f $^4\Pi_g$) $5p\sigma_u$, $^3\Pi_u$)	O(5p, ^{3}P)	$2s^22p^2(^4S^0)4p$, $^3P \rightarrow 2s^22p^2(^4S^0)3s$, $^3S^0$	369.4	369.34
		O_2** ((O_2^+ f $^4\Pi_g$) $5s\sigma_u$, $^3\Pi_u$)	O(5s, ^{5}S^0)	$2s^22p^2(^4S^0)5s$, $^5S^0 \rightarrow 2s^22p^2(^4S^0)3p$, ^5P	645.4	654.44
			O(5s, ^{3}S^0)	$2s^22p^2(^4S^0)5s$, $^3S^0 \rightarrow 2s^22p^2(^4S^0)3p$, ^3P	725.8	725.45
		O_2** ((O_2^+ f $^4\Pi_g$) $6s\sigma_u$, $^3\Pi_u$)	O(6s, ^{5}S^0)	$2s^22p^2(^4S^0)$ 6s, $^5S^0 \rightarrow 2s^22p^2(^4S^0)3p$, ^5P	543.5	543.69
			O(6s, ^{3}S^0)	$2s^22p^2(^4S^0)$ 6s, $^3S^0 \rightarrow 2s^22p^2(^4S^0)3p$, ^3P	604.9	604.65
		O_2** ((O_2^+ f $^4\Pi_g$) $7s\sigma_u$, $^3\Pi_u$)	O(7s, ^{5}S^0)	$2s^22p^2(^4S^0)$ 7s, $^5S^0 \rightarrow 2s^22p^2(^4S^0)3p$, ^5P	502.2	501.88
			O(7s, ^{3}S^0)	$2s^22p^2(^4S^0)$ 7s, $^3S^0 \rightarrow 2s^22p^2(^4S^0)3p$, ^3P	555.6	555.5
		O_2** ((O_2^+ f $^4\Pi_g$) $8s\sigma_u$, $^3\Pi_u$)	O(8s, ^{5}S^0)	$2s^22p^2(^4S^0)$ 8s, $^5S^0 \rightarrow 2s^22p^2(^4S^0)3p$, ^5P	480.4	480.30
			O(8s, ^{3}S^0)	$2s^22p^2(^4S^0)$ 8s, $^3S^0 \rightarrow 2s^22p^2(^4S^0)3p$, ^3P	530.1	529.91
		O_2** ((O_2^+ f $^4\Pi_g$) $9s\sigma_u$, $^3\Pi_u$)	O(9s, ^{5}S^0)	$2s^22p^2(^4S^0)$ 9s,$^5S^0 \rightarrow 2s^22p^2(^4S^0)3p$,$^5P^{\blacktriangle}$	467.6	
19.0−21.0	O_2** ((O_2^+ B $^2\Sigma_g^-$) $np\sigma_u$, $^3\Sigma_u^-$) $n = 4, 5$	O_2** ((O_2^+ f $^4\Pi_g$) $9s\sigma_u$, $^3\Pi_u$)	O(9s, ^{3}S^0)	$2s^22p^2(^4S^0)$ 9s, $^3S^0 \rightarrow 2s^22p^2(^4S^0)3p$,$^3P^{\blacktriangle}$	514.9	
		O_2** ((O_2^+ f $^4\Pi_g$) $10s\sigma_u$, $^3\Pi_u$)	O(10s, ^{5}S^0)	$2s^22p^2(^4S^0)$ 10s,$^5S^0 \rightarrow 2s^22p^2(^4S^0)3p$,$^5P^{\blacktriangle}$	459.1	
			O(10s, ^{3}S^0)	$2s^22p^2(^4S^0)$ 10s,$^3S^0 \rightarrow 2s^22p^2(^4S^0)3p$,$^3P^{\blacktriangle}$	505.4	
		O_2** ((O_2^+ f $^4\Pi_g$) $11s\sigma_u$, $^3\Pi_u$)	O(11s, ^{5}S^0)	$2s^22p^2(^4S^0)$ 11s,$^5S^0 \rightarrow 2s^22p^2(^4S^0)3p$,$^5P^{\blacktriangle\blacktriangle}$	453.4	
		O_2** ((O_2^+ f $^4\Pi_g$) $12s\sigma_u$, $^3\Pi_u$)	O(12s, ^{5}S^0)	$2s^22p^2(^4S^0)$ 12s,$^5S^0 \rightarrow 2s^22p^2(^4S^0)3p$,$^5P^{\blacktriangle\blacktriangle}$	449.1	
		O_2** ((O_2^+ f $^4\Pi_g$) $4d\sigma_u$, $^3\Pi_u$)	O(4d, ^{5}D^0)	$2s^22p^2(^4S^0)$4d, $^5D^0 \rightarrow 2s^22p^2(^4S^0)3p$,$^5P$	615.9	615.82
			O(4d, ^{3}D^0)	$2s^22p^2(^4S^0)$4d, $^3D^0 \rightarrow 2s^22p^2(^4S^0)3p$,$^3P$	700.6	700.22
		O_2** ((O_2^+ f $^4\Pi_g$) $5d\sigma_u$, $^3\Pi_u$)	O(5d, ^{5}D^0)	$2s^22p^2(^4S^0)$ 5d, $^5D^0 \rightarrow 2s^22p^2(^4S^0)3p$,$^5P$	533.2	532.97
			O(5d, ^{3}D^0)	$2s^22p^2(^4S^0)$5d, $^3D^0 \rightarrow 2s^22p^2(^4S^0)3p$,$^3P$	596.2	595.86
		O_2** ((O_2^+ f $^4\Pi_g$) $6d\sigma_u$, $^3\Pi_u$)	O(6d, ^{5}D^0)	$2s^22p^2(^4S^0)$ 6d,$^5D^0 \rightarrow 2s^22p^2(^4S^0)3p$,$^5P$	497.1	496.88
			O(6d, ^{3}D^0)	$2s^22p^2(^4S^0)$6d, $^3D^0 \rightarrow 2s^22p^2(^4S^0)3p$,$^3P$	551.4	551.28
		O_2** ((O_2^+ f $^4\Pi_g$) $7d\sigma_u$, $^3\Pi_u$)	O(7d, ^{5}D^0)	$2s^22p^2(^4S^0)$7d,$^5D^0 \rightarrow 2s^22p^2(^4S^0)3p$, ^5P	477.5	477.38
			O(7d, ^{3}D^0)	$2s^22p^2(^4S^0)$7d, $^3D^0 \rightarrow 2s^22p^2(^4S^0)3p$,$^3P$	527.7	527.65
		O_2** ((O_2^+ f $^4\Pi_g$) $8d\sigma_u$, $^3\Pi_u$)	O(8d, ^{5}D^0)	$2s^22p^2(^4S^0)$8d,$^5D^0 \rightarrow 2s^22p^2(^4S^0)3p$,$^5P$	465.7	465.54
			O(8d, ^{3}D^0)	$2s^22p^2(^4S^0)$8d, $^3D^0 \rightarrow 2s^22p^2(^4S^0)3p$,$^3P$	513.3	513.27
		O_2** ((O_2^+ f $^4\Pi_g$) $9d\sigma_u$, $^3\Pi_u$)	O(9d, ^{5}D^0)	$2s^22p^2(^4S^0)$9d,$^5D^0 \rightarrow 2s^22p^2(^4S^0)3p$,$^5P^{\blacktriangle}$	458.0	
			O(9d, ^{3}D^0)	$2s^22p^2(^4S^0)$9d,$^3D^0 \rightarrow 2s^22p^2(^4S^0)3p$,$^3P^{\blacktriangle}$	503.9	
		O_2** ((O_2^+ f $^4\Pi_g$) $10d\sigma_u$, $^3\Pi_u$)	O(10d, ^{5}D^0)	$2s^22p^2(^4S^0)$10d,$^5D^0 \rightarrow 2s^22p^2(^4S^0)3p$,$^5P^{\blacktriangle}$	452.5	
		O_2** ((O_2^+ f $^4\Pi_g$) $11d\sigma_u$, $^3\Pi_u$)	O(11d, ^{5}D^0)	$2s^22p^2(^4S^0)$11d,$^5D^0 \rightarrow 2s^22p^2(^4S^0)3p$,$^5P^{\blacktriangle\blacktriangle}$	448.5	
19.0−21.0	O_2** ((O_2^+ B $^2\Sigma_g^-$) $np\pi_u$, $^3\Pi_u$) $n = 4, 5$	O_2**(O_2^+ d $^4\Sigma_g^+$) $3p\sigma_u$, $^3\Sigma_u^+$)	O(3p, ^{5}P)	$2s^22p^2(^4S^0)3p$, $^5P \rightarrow 2s^22p^2(^4S^0)3s$, $^5S^0$	777.5	777.54
			O(3p, ^{3}P)	$2s^22p^2(^4S^0)3p$, $^3P \rightarrow 2s^22p^2(^4S^0)3s$, $^3S^0$	845.0	844.68
		O_2**(O_2^+ d $^4\Sigma_g^+$) $4p\sigma_u$,$^3\Sigma_u^+$)	O(4p, ^{5}P)	$2s^22p^2(^4S^0)4p$, $^5P \rightarrow 2s^22p^2(^4S^0)3s$, $^5S^0$	394.8	394.75
			O (4p, ^{3}P)	$2s^22p^2(^4S^0)4p$, $^3P \rightarrow 2s^22p^2(^4S^0)3s$, $^3S^0$	436.8	436.83
		O_2**(O_2^+ d $^4\Sigma_g^+$) $5p\sigma_u$,$^3\Sigma_u^+$)	O(5p, ^{3}P)	$2s^22p^2(^4S^0)4p$, $^3P \rightarrow 2s^22p^2(^4S^0)3s$, $^3S^0$	369.4	369.34
		O_2**(O_2^+ d $^4\Sigma_g^+$) $5s\sigma_u$, $^3\Sigma_u^+$)	O(5s, ^{5}S^0)	$2s^22p^2(^4S^0)5s$,$^5S^0 \rightarrow 2s^22p^2(^4S^0)3p$, ^5P	645.4	654.44
			O(5s, ^{3}S^0)	$2s^22p^2(^4S^0)5s$, $^3S^0 \rightarrow 2s^22p^2(^4S^0)3p$, ^3P	725.8	725.45
19.0−21.0	O_2** ((O_2^+ B $^2\Sigma_g^-$) $np\pi_u$, $^3\Pi_u$) $n = 4, 5$	O_2**(O_2^+ d $^4\Sigma_g^+$) $6s\sigma_u$,$^3\Sigma_u^+$)	O(6s, ^{5}S^0)	$2s^22p^2(^4S^0)$ 6s, $^5S^0 \rightarrow 2s^22p^2(^4S^0)3p$,$^5P$	543.5	543.69
			O(6s, ^{3}S^0)	$2s^22p^2(^4S^0)$ 6s, $^3S^0 \rightarrow 2s^22p^2(^4S^0)3p$,$^3P$	604.9	604.65
		O_2**(O_2^+ d $^4\Sigma_g^+$) $7s\sigma_u$,$^3\Sigma_u^+$)	O(7s, ^{5}S^0)	$2s^22p^2(^4S^0)$ 7s, $^5S^0 \rightarrow 2s^22p^2(^4S^0)3p$,$^5P$	502.2	501.88
			O(7s, ^{3}S^0)	$2s^22p^2(^4S^0)$ 7s, $^3S^0 \rightarrow 2s^22p^2(^4S^0)3p$,$^3P$	555.6	555.5
		O_2**(O_2^+ d $^4\Sigma_g^+$) $8s\sigma_u$, $^3\Sigma_u^+$)	O(8s, ^{5}S^0)	$2s^22p^2(^4S^0)$ 8s, $^5S^0 \rightarrow 2s^22p^2(^4S^0)3p$,$^5P$	480.4	480.30
			O(8s, ^{3}S^0)	$2s^22p^2(^4S^0)$ 8s, $^3S^0 \rightarrow 2s^22p^2(^4S^0)3p$,$^3P$	530.1	529.91
		O_2**(O_2^+ d $^4\Sigma_g^+$) $9s\sigma_u$,$^3\Sigma_u^+$)	O(9s, ^{5}S^0)	$2s^22p^2(^4S^0)$ 9s, $^5S^0 \rightarrow 2s^22p^2(^4S^0)3p$,$^5P^{\blacktriangle}$	467.6	
			O(9s, ^{3}S^0)	$2s^22p^2(^4S^0)$ 9s, $^3S^0 \rightarrow 2s^22p^2(^4S^0)3p$,$^3P^{\blacktriangle}$	514.9	
		O_2**(O_2^+ d $^4\Sigma_g^+$)10sσ_u, $^3\Sigma_u^+$)	O(10s,^{5}S^0)	$2s^22p^2(^4S^0)$ 10s, $^5S^0 \rightarrow 2s^22p^2(^4S^0)3p$, $^5P^{\blacktriangle}$	459.1	
			O(10s, ^{3}S^0)	$2s^22p^2(^4S^0)$ 10s, $^3S^0 \rightarrow 2s^22p^2(^4S^0)3p$,$^3P^{\blacktriangle}$	505.4	
		O_2**(O_2^+ d $^4\Sigma_g^+$) 11sσ_u,$^3\Sigma_u^+$)	O(11s, ^{5}S^0)	$2s^22p^2(^4S^0)$ 11s,$^5S^0 \rightarrow 2s^22p^2(^4S^0)3p$,$^5P^{\blacktriangle\blacktriangle}$	453.4	
		O_2**(O_2^+ d $^4\Sigma_g^+$) 12sσ_u,$^3\Sigma_u^+$)	O(12s, ^{5}S^0)	$2s^22p^2(^4S^0)$ 12s,$^5S^0 \rightarrow 2s^22p^2(^4S^0)3p$,$^5P^{\blacktriangle\blacktriangle}$	449.1	
		O_2**(O_2^+ d $^4\Sigma_g^+$) 4dσ_u, $^3\Sigma_u^+$)	O(4d, ^{5}D^0)	$2s^22p^2(^4S^0)$4d,$^5D^0 \rightarrow 2s^22p^2(^4S^0)3p$,$^5P$	615.9	615.82
			O(4d, ^{3}D^0)	$2s^22p^2(^4S^0)$4d, $^3D^0 \rightarrow 2s^22p^2(^4S^0)3p$,$^3P$	700.6	700.22
		O_2**(O_2^+ d $^4\Sigma_g^+$) 5dσ_u, $^3\Sigma_u^+$)	O(5d, ^{5}D^0)	$2s^22p^2(^4S^0)$5d,$^5D^0 \rightarrow 2s^22p^2(^4S^0)3p$,$^5P$	533.2	532.97
			O(5d, ^{3}D^0)	$2s^22p^2(^4S^0)$5d, $^3D^0 \rightarrow 2s^22p^2(^4S^0)3p$,$^3P$	596.2	595.86
		O_2**(O_2^+ d $^4\Sigma_g^+$) 6dσ_u,$^3\Sigma_u^+$)	O(6d, ^{5}D^0)	$2s^22p^2(^4S^0)$6d,$^5D^0 \rightarrow 2s^22p^2(^4S^0)3p$,$^5P$	497.1	496.88

TABLE 1: Continued

excitation energy (eV)	SESs OES	SESs DES	dissociation products	assignments of transitions	emission wavelengths (nm) Observation	emission wavelengths (nm) ref 20
			O(6d, $^3D^0$)	$2s^22p^2(^4S^0)6d, {}^3D^0 \rightarrow 2s^22p^2(^4S^0)3p, {}^3P$	551.4	551.28
		$O_2{}^{**}((O_2{}^+ d\ {}^4\Sigma_g{}^+)\ 7d\sigma_u, {}^3\Sigma_u{}^+)$	O(7d, $^5D^0$)	$2s^22p^2(^4S^0)7d, {}^5D^0 \rightarrow 2s^22p^2(^4S^0)3p, {}^5P$	477.5	477.38
			O(7d, $^3D^0$)	$2s^22p^2(^4S^0)7d, {}^3D^0 \rightarrow 2s^22p^2(^4S^0)3p, {}^3P$	527.7	527.65
		$O_2{}^{**}((O_2{}^+ d\ {}^4\Sigma_g{}^+)\ 8d\sigma_u, {}^3\Sigma_u{}^+)$	O(8d, $^5D^0$)	$2s^22p^2(^4S^0)8d, {}^5D^0 \rightarrow 2s^22p^2(^4S^0)3p, {}^5P$	465.7	465.54
			O(8d, $^3D^0$)	$2s^22p^2(^4S^0)8d, {}^3D^0 \rightarrow 2s^22p^2(^4S^0)3p, {}^3P$	513.3	513.27
		$O_2{}^{**}((O_2{}^+ d\ {}^4\Sigma_g{}^+)\ 9d\sigma_u, {}^3\Sigma_u{}^+)$	O(9d, $^5D^0$)	$2s^22p^2(^4S^0)9d, {}^5D^0 \rightarrow 2s^22p^2(^4S^0)3p, {}^5P^{\blacktriangle}$	458.0	
			O(9d, $^3D^0$)	$2s^22p^2(^4S^0)\ 9d, {}^5D^0 \rightarrow 2s^22p^2(^4S^0)3p, {}^3P^{\blacktriangle}$	503.9	
		$O_2{}^{**}((O_2{}^+ d\ {}^4\Sigma_g{}^+)\ 10d\sigma_u, {}^3\Sigma_u{}^+)$	O(10d, $^5D^0$)	$2s^22p^2(^4S^0)\ 10d, {}^5D^0 \rightarrow 2s^22p^2(^4S^0)3p, {}^5P^{\blacktriangle}$	452.5	
		$O_2{}^{**}((O_2{}^+ d\ {}^4\Sigma_g{}^+)\ 11d\sigma_u, {}^3\Sigma_u{}^+)$	O(11d, $^5D^0$)	$2s^22p^2(^4S^0)\ 11d, {}^5D^0 \rightarrow 2s^22p^2(^4S^0)3p, {}^5P^{\blacktriangle\blacktriangle}$	448.5	

[a] Ten new Rydberg transitions are marked by a single triangle. The transitions referred to three new Rydberg states are marked by double triangles.

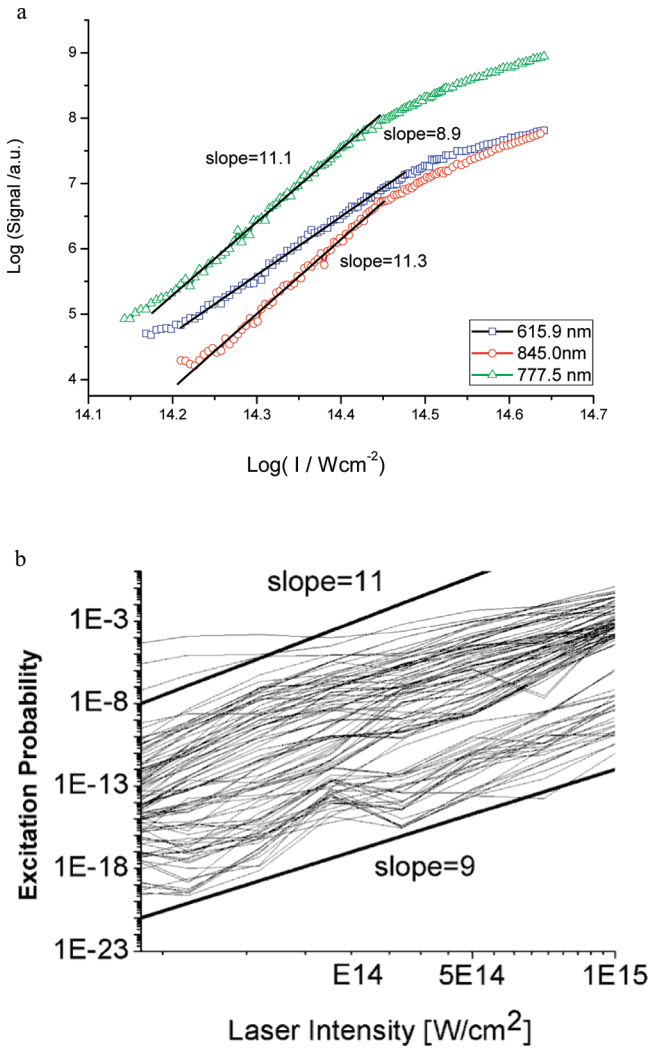

Figure 4. (a) Fluorescence intensity dependence on the laser intensity. The fluorescence is collected and integrated around 615.9, 777.5 and 845.0 nm, respectively. They are transitions of $2s^22p^2(^4S^0)4d, {}^5D^0 \rightarrow 2s^22p^2(^4S^0)3p, {}^5P$, $2s^22p^2(^4S^0)3p, {}^5P \rightarrow 2s^22p^2(^4S^0)3s, {}^5S^0$, and $2s^22p^2(^4S^0)3s, {}^3P \rightarrow 2s^22p^2(^4S^0)3s, {}^3S^0$. (b) Excitation probabilities to various excited states of O_2 as functions of laser intensity. Here, the laser pulse duration time is 42 fs, and the central frequencies of the laser pulse are 800 nm.

results. It indicates that the O_2 molecule dissociates into O excited atomic products via its highly excited states. It should be noted here that only the molecules in SESs states can dissociate, because the threshold production of fragments (O (ground state) + O (Rydberg state)) is at least 15 eV.

SESs of molecules are created in the excitation process. These superexcited molecules decay into the various channels "spontaneously".

3.3. Morse PECs of the SESs. Dissociation takes place in the SESs of oxygen molecule. To understand the dissociation mechanism, the PESs of the SESs should be understood at first. However, there is lack of quantum-mechanically calculated results for SESs so far, even for diatomic molecules like O_2. In this section, we first make an empirical PECs for the SESs. In light of these empirical (Morse type) PECs, we further interpret the dissociation processes.

3.3.1. Symbol of the SESs. Following Hatano,[4,5] we interpret the SESs as those appropriately excited Rydberg states. We shall start by proposing a spectroscopic nomenclature of such states. Quantitative justification of such interpretation through PES calculation and comparison with experimental results will follow.

The SES of a molecule M is expressed as a symbol M** followed by a more specific molecular notation ((M^+, spectral term of the ion to which the Rydberg states converges) $nl\lambda$, spectral term of the molecule). For example, $O_2{}^{**}$ (($O_2{}^+$ a $^4\Pi_u$) $4s\sigma_g$, $^3\Pi_u$) denotes a specific SES of oxygen molecule. In this case, the double asterisk means a superexcited state which possesses energy higher than the first IP. The SES is the Rydberg state converging to the excited state (a $^4\Pi_u$) of $O_2{}^+$ ion. The principle quantum number n, the angular quantum number l, and its projection onto the molecular axis λ of the molecule in the Rydberg series, are indicated by the symbols 4, s, and σ, respectively. Finally, the Rydberg state has a spectral term of $^3\Pi_u$.

3.3.2. Morse PECs of the SESs. Among the empirical functions, the Morse function is the most explicit one. The Morse function denotes the potential energy $V(r)$ of the molecule as a function of the bond distance r

$$V_e = D_e(e^{-2a(r-r_e)} - 2e^{-a(r-r_e)}) \quad (1)$$

where D_e is the depth of the potential well and r_e is equilibrium bond distance. The symbol a is the Morse parameter.

The vibrational frequency ω_e and the equilibrium bond distance r_e of the Rydberg states are adapted from those of the O_2 ions to which they converge. It is based on the ionic core approximation, which treats the Rydberg molecules as an ion. The depth of the potential well, D_e, consists of two parts, the zero point energy E_0 and the dissociation energy D_0. D_0 is the difference between the energy of the Rydberg O_2 molecule E_r and that of the products of O + O* (in Rydberg states) E_p, i.e., $D_0 = E_p - E_r$. The data of E_p are adapted from the NIST table.[22] E_r is obtained by the formula $E_r = IP - R/(n - \delta)^2$, where δ is the quantum defect and R is Rydberg constant.

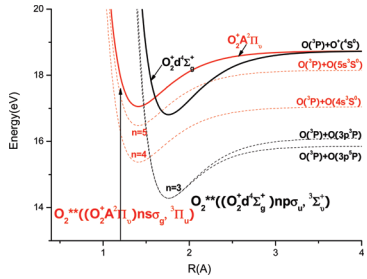

Figure 5. PECs of the SESs series of $O_2^{**}((O_2^+ A\ ^2\Pi_u)\ ns\sigma_g, {}^3\Pi_u)$ and $O_2^{**}((O_2^+ d\ ^4\Sigma_g^+)\ np\sigma_u, {}^3\Sigma_u^+)$. The solid and dash lines show ionic states and SESs, respectively.

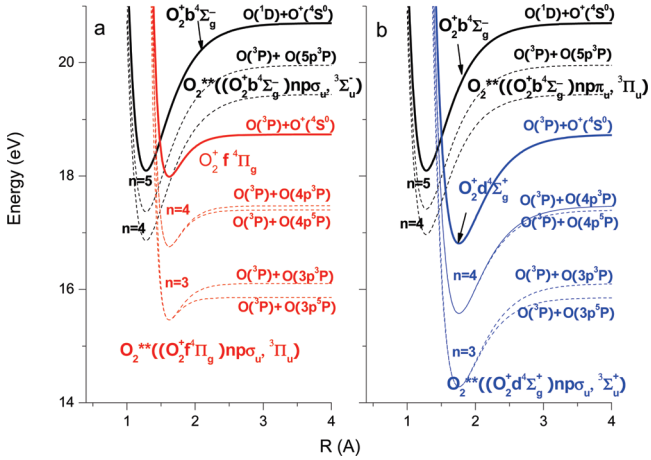

Figure 6. PECs of the SESs series of (a) O_2^{**} $((O_2^+ b\ ^4\Sigma_g^-)\ np\sigma_u, {}^3\Sigma_u^-)$ and O_2^{**} $((O_2^+ f\ ^4\Pi_u)\ np\sigma_u, {}^3\Pi_u)$ and (b) O_2^{**} $((O_2^+ b\ ^4\Sigma_g^-)\ np\pi_u, {}^3\Pi_u)$ and O_2^{**} $((O_2^+ d\ ^4\Sigma_g^+)\ np\sigma_u, {}^3\Sigma_u^+)$. The solid and dash lines show ionic states and SESs, respectively.

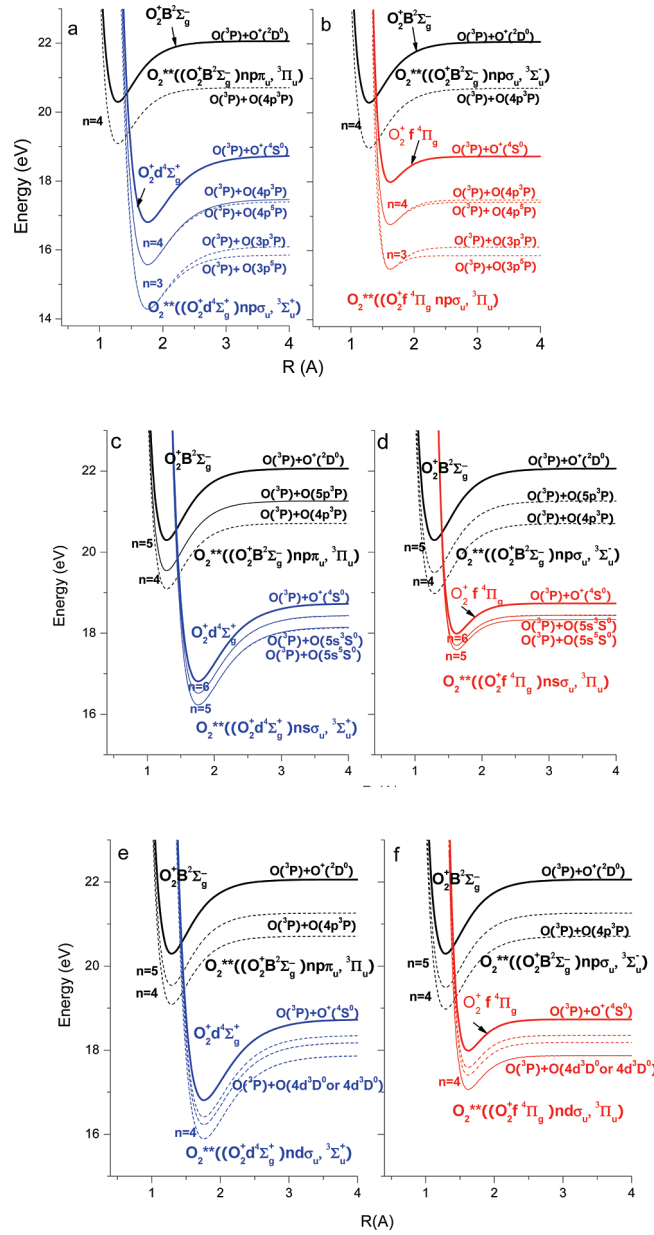

Figure 7. PECs of the SESs series of (a) O_2^{**} $((O_2^+ B\ ^2\Sigma_g^-)\ np\sigma_u, {}^3\Sigma_u^-)$ and O_2^{**} $((O_2^+ f\ ^4\Pi_u)\ np\sigma_u, {}^3\Pi_u)$, (b) O_2^{**} $((O_2^+ B\ ^2\Sigma_g^-)\ np\pi_u, {}^3\Pi_u)$ and O_2^{**} $((O_2^+ d\ ^4\Sigma_g^+)\ np\sigma_u, {}^3\Sigma_u^+)$, (c) O_2^{**} $((O_2^+ B\ ^2\Sigma_g^-)\ np\pi_u, {}^3\Pi_u)$ and O_2^{**} $((O_2^+ d\ ^4\Sigma_g^+)\ ns\sigma_u, {}^3\Sigma_u^+)$, (d) O_2^{**} $((O_2^+ B\ ^2\Sigma_g^-)\ np\sigma_u, {}^3\Sigma_u^-)$ and O_2^{**} $((O_2^+ f\ ^4\Pi_u)\ ns\sigma_u, {}^3\Pi_u)$, (e) O_2^{**} $((O_2^+ B^2\Sigma_g^-)\ np\pi_u, {}^3\Pi_u)$ and O_2^{**} $((O_2^+ d\ ^4\Sigma_g^+)\ nd\sigma_u, {}^3\Sigma_u^+)$, and (f) O_2^{**} $((O_2^+ B\ ^2\Sigma_g^-)\ np\sigma_u, {}^3\Sigma_u^-)$ and O_2^{**} $((O_2^+ f\ ^4\Pi_u)\ nd\sigma_u, {}^3\Pi_u)$. The solid and dashed lines show ionic states and SESs, respectively.

To our knowledge, the correlation between the quantum numbers of high-Rydberg molecules and those of these Rydberg fragments is an unsolved problem. We thus assume that the principle quantum number (n) and the angular quantum number (l) do not change in the dissociation processes to correlate a specific PEC with its dissociation products. Our assumption is supported by the following well-known point: "If the core ion is formed in a sufficiently high excited state, it can dissociate with no help from the high-Rydberg electron. The fragments can separate to an appreciate distance and still remain completely within the high-Rydberg orbital".[23] Therefore, the possible products in the dissociation are shown on the right-hand side of the curves in Figures 5−7. For example, in Figure 5, $O_2^{**}((O_2^+ A\ ^2\Pi_u)\ 4s\sigma_g, {}^3\Pi_u)$ can dissociate into two atoms, a ground state O atom (^3P) and a Rydberg atom O (4s, $^3S^0$).

With eq 1, we have built the Morse type PECs for the SESs of oxygen molecules. The PECs are shown as the curves in Figures 5−7. Each figure depicts two series of Rydberg states with different principle quantum numbers n. It can be seen in the figure that there are two types of curves, featured by different equilibrium distances and different depths of the potential well.

The first type of PECs has short equilibrium bond distances about 1.30 Å, which is comparable to that of the ground state, 1.21 Å. The corresponding SESs converge to the A ($^2\Pi_u$), b ($^4\Sigma_g^-$), and B ($^2\Sigma_g^-$) states of O_2^+ ion. The removed valence electron in the excitation is a nonbonding electron of the molecules. Such excitation does not weaken the chemical bond, so that the potential well is deep. Usually, a vertical excitation from the ground state of O_2 to the kind of SES will create a low vibrationally excited molecule but will not lead to dissociation.

For the second type of PECs, the equilibrium bond distances could be as long as about 1.7 Å. Doubly excited electrons make the O−O bond weaker. These SESs correspond to Rydberg states converging to the ionic states of O_2^+ (d $^4\Sigma_g^+$) or O_2^+ (f $^4\Pi_g$). The potential wells of the PECs are shallow, so that the states are less stable.

3.4. Predissociation Mechanism. Here we discuss some possible dissociation processes of the typical dissociation channels. As shown in Figures 5−7, the SESs are created through the vertical excitation of the first type of Rydberg states. The SESs are low vibrationally excited, which do not lead to

dissociation directly. However, via curve crossing, these SESs can transit to the second type of PECs of SESs, O_2**($(O_2^+$ d $^4\Sigma_g^+$) npσ_u, $^3\Sigma_u^+$), O_2** ($(O_2^+$ f $^4\Pi_g$) npσ_u, $^3\Pi_u$), O_2** ($(O_2^+$ f $^4\Pi_g$) nsσ_u, $^3\Pi_u$), O_2**($(O_2^+$ d $^4\Sigma_g^+$) nsσ_u, $^3\Sigma_u^+$), O_2** ($(O_2^+$ f $^4\Pi_g$) ndσ_u, $^3\Pi_u$), and O_2**($(O_2^+$ d $^4\Sigma_g^+$) ndσ_u, $^3\Sigma_u^+$) series.[17,24,25] This transition usually produces highly vibrational excitation in these SESs. The vibrationally hot molecules thus would undergo dissociation. In other words, predissociation of the O_2 molecule takes place via these superexcited states.

The variety of the fluorescence emissions in the experiment indicate that many predissociation channels occur. In light of the Morse PECs shown in Figures 5−7, we are able to understand all these predissociation processes. Table 1 summaries the excitation energy, the optically excited state, the dissociative state, the possible products and the product emissions of each dissociation process.

3.4.1. SESs of O_2** ($(O_2^+$ A $^2\Pi_u$) nsσ_g, $^3\Pi_u$) States. In the energy region of 15.3−17.1 eV, a Franck−Condon excitation may create the Rydberg states of $n = 4$, 5 of the nsσ_g series converging to the A $^2\Pi_u$ state of O_2^+ ion. These SESs are stable and do not undergo dissociation directly. The stability energies of the states are 1.70 and 1.67 eV, respectively (Figure 5). However, it can be seen in Figure 5 that these Rydberg states can transit to the SES of O_2**($(O_2^+$ d $^4\Sigma_g^+$) 3pσ_u, $^3\Sigma_u^+$) via curve crossing. The transition results in a highly vibrational excitation in the latter state. The hot O_2**($(O_2^+$ d $^4\Sigma_g^+$) 3pσ_u, $^3\Sigma_u^+$) thus undergoes predissociation, leading to the products of O (^{3}P) + O(3p, ^{5}P) or O (^{3}P) + O(3p, ^{3}P). The production of O(3p, ^{5}P) and O(3p, ^{3}P) is verified by the emissions at 777.5 and 845.0 nm, which are assigned to the transitions of O(3p, ^{5}P → 3s, ^{5}S^0) and O(3p, ^{3}P → 3s, ^{3}S^0), respectively.

3.4.2. SESs of O_2** ($(O_2^+$ b $^4\Sigma_g^-$) npπ_u, $^3\Pi_u$) and O_2** ($(O_2^+$ b $^4\Sigma_g^-$) npσ_u, $^3\Sigma_u^-$) States. At a higher excitation energy of 17.0 eV, Rydberg states of O_2** ($(O_2^+$ b $^4\Sigma_g^-$) 4pπ_u, $^3\Pi_u$) and O_2** ($(O_2^+$ b $^4\Sigma_g^-$) 4pσ_u, $^3\Sigma_u^-$) can be produced by the vertical excitation directly (Figure 6a,b). These Rydberg states of O_2 molecule cross to two other SESs of O_2** ($(O_2^+$ d $^4\Sigma_g^+$) 3pσ_u, $^3\Sigma_u^+$) or O_2** ($(O_2^+$ f $^4\Pi_g$) 3pσ_u, $^3\Pi_u$) individually. The transition via the curve crossing creates a highly vibrational excitation in the latter two states. The hot O_2 molecule thus undergoes dissociation. The products are O (^{3}P) + O (3p, ^{5}P) or O (^{3}P) + O (3p, ^{3}P). The observed emissions at 777.5 and 845.0 nm refer to the transitions of O(3p, ^{5}P → 3s, ^{5}S^0) and O(3p, ^{3}P → 3s, ^{3}S^0), respectively.

At a higher excitation of 17.5 eV, O_2** ($(O_2^+$ b $^4\Sigma_g^-$) 5pσ_u, $^3\Sigma_u^-$) and O_2** ($(O_2^+$ b $^4\Sigma_g^-$) 5pπ_u, $^3\Pi_u$) states may be created in the laser excitation (Figure 6a,b). These SESs cross with the O_2** ($(O_2^+$ f $^4\Pi_g$) 4pσ_u, $^3\Pi_u$) and O_2** ($(O_2^+$ d $^4\Sigma_g^+$) 4pσ_u, $^3\Sigma_u^+$) states, respectively. The latter two states further dissociate, leading to the products of O (^{3}P) + O(4p, ^{5}P) or O (^{3}P) + O(4p, ^{3}P), which emit the fluorescent lights at 394.8 nm or 436.8 nm, respectively.

3.4.3. SESs of O_2**($(O_2^+$ B $^2\Sigma_g^-$) npπ_u, $^3\Pi_u$) and O_2**($(O_2^+$ B $^2\Sigma_g^-$) npσ_u, $^3\Sigma_u^-$) States. At a higher excitation energy of 19.0 eV, Rydberg states of O_2** ($(O_2^+$ B $^2\Sigma_g^-$) 4pπ_u, $^3\Pi_u$) and O_2** ($(O_2^+$ B $^2\Sigma_g^-$) 4pσ_u, $^3\Sigma_u^-$) can be produced by the optical excitation (Figure 7). The SESs cross to the O_2** ($(O_2^+$ d $^4\Sigma_g^+$) 3pσ_u, $^3\Sigma_u^+$) or O_2** ($(O_2^+$ f $^4\Pi_g$) 3pσ_u, $^3\Pi_u$) states, producing the fragments of O (3p, ^{3}P) and O (3p, ^{5}P) (Figure 7a,b). Meanwhile, the SESs cross to the O_2** ($(O_2^+$ d $^4\Sigma_g^+$) 5sσ_u, $^3\Sigma_u^+$) and O_2** ($(O_2^+$ f $^4\Pi_g$) 5sσ_u, $^3\Pi_u$) also, producing O (5s, ^{5}S^0) or (5s, ^{3}S^0) (Figure 7c,d). The observed emissions at 645.4 and 725.8 nm refer to the transitions of O (5s, ^{5}S^0 → 3p, ^{5}P) and O (5s, ^{3}S^0 → 3p, ^{3}P), respectively. And the SESs will also cross to the O_2** ($(O_2^+$ d $^4\Sigma_g^+$) 4dσ_u, $^3\Sigma_u^+$) and O_2** ($(O_2^+$ f $^4\Pi_g$) 4dσ_u, $^3\Pi_u$), leading to the products of O (4d, ^{5}D^0) and O (4d, ^{3}D^0) (Figure 7e,f). The observed emission at 615.9 nm and 700.6 nm refers to the transitions of O (4d, ^{5}D^0 → 3p, ^{5}P) and O (4d, ^{3}D^0 → 3p, ^{3}P), respectively. Such observations verify the predissociation mechanism.

3.5. Dissociation Dynamics. ***3.5.1. Dissociation Period Predicted by QCT Calculations.*** The predissociation process consists of two steps. The first step can be represented by a wave packet moving on the first type of PEC before the curve crossing (Figure 5). In the second step, the wave packet transits across the crossing point, resulting in a highly vibrational excitation in the second type of PEC. The wave packet moves on the latter PEC further, leading to the products of two oxygen atoms.

QCT calculations are carried out for the first step. A Gaussian wave packet in Wigner representation starts to move on the PEC with an average zero initial velocity.[26] According to Franck−Condon principle, the initial geometry is adapted as that of the ground state of O_2 molecule, which has a short bond distance of 1.21 Å. The wave packet is then accelerated by the repulsive force on the left wall of the PEC. Trajectories reflecting the moving time of the wave packet on the state of O_2** ($(O_2^+$ b $^4\Sigma_g^-$) 4pπ_u, $^3\Pi_u$) are calculated. Figure 8a shows the calculated probability of the trajectories of the SES moving toward and reaching the crossing point as a function of time. The width of the curve indicates that the average moving time to the crossing point is about 100 fs. Otherwise, if it was a direct dissociation, the dissociation period would be as long as about 600 fs predicted in a similar calculation. Autoionization process of SESs for O_2 molecule is not considered in this work. They are often estimated to be $10^{10}n^{-3}$ to $10^{12}n^{-3}$ s^{-1} (n means principal quantum number). For a Rydberg molecule of $n = 4$, the autoionization lifetime is thus subnanoseconds,[23] much longer than the neutral dissociation time of SES.

3.5.2. Fluorescence Depletion Experiment. The crossing time of the initially excited SESs to the final dissociating PEC is inspected by an experiment using femtosecond lasers. On the basis of the above analysis, if during the crossing period, the initially excited SES population is reduced by a weak probe ultrashort laser pulse, the resultant fluorescence would be reduced. It is predicted that the fluorescence reduction time would be on the order of 100 fs (see Figure 8a), corresponding to the transit time between the initial SES and the final dissociating SES as obtained in the previous section. Once the crossing to the second type of SES is over, the weak probe pulse would not be able to de-excite the dissociating SES or Rydberg state.

To monitor the dissociation process of the SESs, two sequential ultrafast laser pulses at different wavelengths have been employed. The time interval between the two laser pulses is varied in the experiment. The first (pump) laser pulse initiates the multiphoton excitation, creating a SES of the first type of PEC. The second (probe) laser pulse depopulates the SES either by further excitation or by spontaneous emission pumping (SEP). The depopulation of the superexcited states results in a decrease of product yields which causes a depletion of fluorescence emission. The fluorescence intensity has been measured as a function of the delay time between the pump and the probe laser pulses.

Figure 8b shows the fluorescence signals at 777.5 nm as a function of the delay time, respectively. It can be seen clearly that an obvious depletion of the fluorescence signal appears

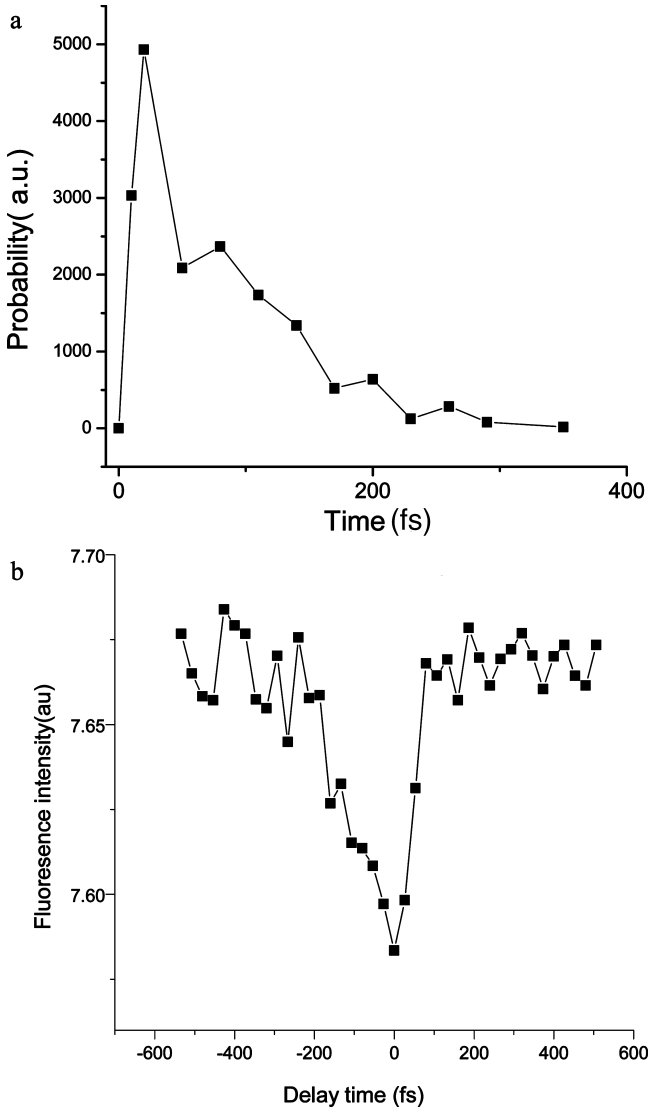

Figure 8. (a) Probability of the trajectories for O_2** ((O_2^+ b $^4\Sigma_g^-$) 4pπ_u, $^3\Pi_u$) moving to the crossing point as a function of time. (b) Integrated fluorescence signal of $2s^22p^2(^4S^0)3p,^5P \rightarrow 2s^22p^2(^4S^0)3s,^5S^0$ at 777.5 nm versus the delay time between the pump and probe pulses. Negative delay time means the probe pulses are behind the pump pulses.

when the pump and probe pulses overlap together. The maximum of the depletion is at the zero delay time. The rise time of the depletion is about 50 fs, which is the order of the laser pulse width. The decay lasts for 150 fs. The experimentally recorded curves shown in Figure 8b are analogous to the QCT calculated one shown in Figure 8a. The results support that it is the predissociation process. Similar depletion curves of fluorescence depletion were also observed for the other wavelengths with roughly the same temporal width.

4. Summary and Conclusion

We find that oxygen molecule undergoes neutral dissociation in strong laser fields at the intensity of 2×10^{14} W/cm^2. Thirty-three emission lines have been recorded in the fluorescence spectroscopy. These emissions are caused by the excited oxygen atoms, which are the dissociation products of the oxygen molecules. Ten of them are the new Rydberg transitions, which have not been reported. Three new Rydberg states, $2s^22p^2$ ($^4S^0$)11s,$^5S^0$, $2s^22p^2$ ($^4S^0$)12s, $^5S^0$, and $2s^22p^2(^4S^0)$10d, $^5D^0$, are identified for the first time.

Laser power dependence of the fluorescence intensity shows that each oxygen molecule absorbs ten laser photons on an average. The total energy absorbed is about 15.5 ± 1.5 eV, which is higher than the first ionization potential (IP) of the molecule. This is an alternative method to prepare SESs as compared to the conventional method of SR excitation. After the multiphoton excitation, the superexcited O_2 molecules undergo spontaneous dissociation. To understand the dissociation mechanism of the SESs of O_2 molecules, Morse PECs for different SESs are built and shown in Figures 5−7. Predissociation mechanism is suggested to explain the O−O bond cleavage. A vertical excitation of the ground state O_2 molecule creates the SESs converging to the O_2^+ (A $^2\Pi_u$), O_2^+ (b $^4\Sigma_g^-$), or O_2^+ ($B^2\Sigma_g^-$) ions. These SESs further transit to the other SESs converging to the O_2^+ (f $^4\Pi_g$) or O_2^+ (d $^4\Sigma_g^+$) ions. Finally, the latter states undergo dissociation.

An ultrafast laser diagnostic experiment is performed for O_2 dissociation. A second laser pulse is employed to deplete the fluorescence intensity. The measured lifetime of 150 fs for the intermediate is consistent with predissociation mechanism. QCT calculation shows that the predissociation process requires a short time of about 100 fs while direct dissociation needs a much longer time of 600 fs.

Acknowledgment. This work was supported by the China Ministry of Science and Technology with the Project for Fundamental Research (2006CB806000). The experimental work using femtosecond lasers in Laval University, Canada, was partially supported by NSERC, Canada Research Chairs, CIPI, DRDC-Valcartier and FQRNT.

References and Notes

(1) Inokuti, M. *Radiat. Phys. Chem.* **2001**, *60*, 283.
(2) Platzman, R. L. *Radiat. Res.* **1962**, *17*, 419.
(3) Platzman, R. L. *Vortex* **1962**, *23*, 372.
(4) Hatano, Y. *Radiat. Environ. Biophys.* **1999**, *38*, 239.
(5) Hatano, Y. *Phys. Rep.* **1999**, *313*, 109.
(6) Mason, N. J.; Newell, W. R. *J. Phys. B: At. Mol. Opt. Phys.* **1990**, *23*, 4641.
(7) Borst, W. L.; Zipf, E. C. *Phys. Rev. A* **1971**, *4*, 153.
(8) Suzuki, S.; Mitsuke, K.; Imamura, T.; Koyano, I. *J. Chem. Phys.* **1992**, *96*, 7500.
(9) Hatano, Y. *J. Electron Spectrosc. Relat. Phenom.* **2001**, *119*, 107.
(10) Latimer, C. J.; Mackie, R. A.; Sands, A. M.; Kouchi, N.; Dunn, K. F. *J. Phys. B: At. Mol. Opt. Phys.* **1999**, *32*, 2667.
(11) Kong, F.; Luo, Q.; Xu, H. L.; Sharifi, M.; Song, D.; Chin, S. L. *J. Chem. Phys.* **2006**, *125*, 133320.
(12) Kong, F.; Chin, S. L. *Progress in ultrafast laser science III*; Yamanouchi, K., Chin, S. L., Agostini, P., Ferrante, G., Eds.; 2008; Chapter 6.
(13) Ukai, M.; Machida, S.; Kameta, K.; Kitajima, M.; Kouchi, N.; Hatano, Y.; Ito, K. *Phys. Rev. Lett.* **1995**, *74*, 239.
(14) Romanescu, C.; Manzhos, S.; Boldovsky, D.; Clarke, J.; Loock, H. P. *J. Chem. Phys.* **2000**, *120*, 767.
(15) Azarm, A.; Xu, H. L.; Kamali, Y.; Bernhardt, J.; Song, D.; Xia, A.; Teranishi, Y.; Lin, S. H.; Kong, F.; Chin, S. L. *J. Phys. B: At. Mol. Opt. Phys.* **2008**, *41*, 225601.
(16) Ukai, M.; Kouchi, N.; Kameta, K.; Terazawa, N.; Chikahiro, Y.; Hatano, Y. *Chem. Phys. Lett.* **1992**, *195*, 298.
(17) Karawajczyk, A.; Erman, P.; Rachlew-Kallne, E.; Riu, J. R. I.; Stankiewicz, M.; Franzen, K. Y.; Veseth, L. *Phys. Rev. A* **2000**, *61*, 032718.
(18) Odagiri, T.; Miyagi, H.; Murata, M.; Fukuzawa, H.; Kurokawa, M.; Kitajima, M.; Kouchi, N. *J. Phys. B: At. Mol. Opt. Phys.* **2009**, *42*, 055101.
(19) Robert, Wu. C. Y.; Phillips, E.; Lee, L. C.; Judge, D. L. *J. Chem. Phys.* **1979**, *71*, 769.
(20) Ralchenko, Yu.; Kramida, A. E.; Reader, J.; NIST ASD Team.; *NIST Atomic Spectra Database*, version 3.1.5; 2008; http://physics.nist.gov/asd3. Wiese, W. L.; Fuhr, J. R.; Deters, T. M. *J. Phys. Chem. Ref. Data* **1996**, Monograph No. 7.

(21) Teranishi, Y.; Hayashi, M.; Kong, F.; Chin, S. L.; Chao, S. D.; Mineo, H.; Lin, S. H. *Mol. Phys.* **2008**, *106*, 333.
(22) http://webbook.nist.gov/chemistry/form-ser.html.
(23) Freund, Robert S. *Rydberg states of atoms and molecules* Tebbings, R. F. S., Dunning, F. B., Eds.; Cambridge University Press: Cambridge, U.K., 1983; Chapter 10.
(24) Moseley, J. T.; Cosby, P. C.; Ozene, J. B.; Durup, J. *J. Chem. Phys.* **1979**, *70*, 1474.
(25) Ehresmann, A.; Liebel, H.; Schmoranzer, H.; Wilhelmi, O.; Zimmermann, B.; Schartner, K. H. *J.Phys. B: At. Mol. Opt. Phys.* **2004**, *37*, 389.
(26) Wang, S. F.; Tang, X. P.; Gao, L. R.; Elshakre, M. E.; Kong, F. A. *J. Phys.Chem. A* **2003**, *107*, 6123.

JP907662Z